Scaling of size, shape and surface roughness in Antarctic krill swarms

Alexey B. Ryabov[1] & Geraint A. Tarling[2*]

1. Institute for Chemistry and Biology of the Marine Environment, University of Oldenburg, 26111 Oldenburg, Germany
2. British Antarctic Survey, Natural Environment Research Council, High Cross, Madingley Rd, Cambridge, CB3 0ET, UK

*corresponding author (gant@bas.ac.uk)

Abstract

Antarctic krill are obligate swarmers and the size and shape of the swarms they form can have a major influence on trophic interactions and biogeochemical fluxes in the Southern Ocean. Parameterising variability in size and shape is therefore a useful step towards understanding the operation of the Southern Ocean ecosystem. We analyse the relationships between the length L, thickness T, perimeter P and area A of 4650 vertical cross-sections of open-ocean krill swarms obtained within the Atlantic sector of the Southern Ocean during a summer survey in 2003. Our data shows that these parameters are tightly interrelated. The thickness T increases on average as $L^{0.67}$ and has a log-normal distribution within each length class. The perimeter and area scale with L and T as $P \sim L^{0.77}T$ and $A \sim L^{0.86}T^{0.48}$. The swarm aspect ratio, T/L, decreases approximately as $L^{-0.31}$. The surface roughness (defined as P/A) has a weak dependence on swarm length and decreases approximately as $T^{-0.46}$, which can be explained only by the appearance of indentations and cavities in the swarm shape that elongate the perimeter but do not change the area. Overall, our study finds that there are distinct limits to the size and shape of swarms that Antarctic krill appear to be capable of forming. Using this limits we have classified swarms into 4 types: *Ellipsoidal*, *Filamentous, Needle-*

like and *Indented*. We consider the potential explanatory factors contributing to these limitations and suggest ways in which they can be further explored.

Keywords: acoustics, area, perimeter, aspect ratio, *Euphausia superba*, Scotia Sea, Southern Ocean

Introduction

Swarms of Antarctic krill (hereon: krill) vary enormously from lengths of just a few metres to several kms and vertical thicknesses of over 100 m (Siegel and Kalinowski 1994, Tarling *et al*. 2009, Krafft *et al*. 2012). These variations are accompanied by corresponding changes in other parameters, such as perimeter and area in two dimensions, and surface area and volume in three dimensions, which together define external swarm shape. The shape of a swarm is a function of the summed individual response to the environment, influenced by the responses of neighbours (Parrish and Edelstein-Keshet 1999). The scale of the swarm is also influential on the relative balance of behaviour and physical drivers on ultimate swarms shape (Folt and Burns 1999). Over large scales (swarms of the order of 100 to 10000 m length), behavioural processes (e.g. migration) are believed to combine with physical processes (turbulence, currents and eddies) to generate heterogeneity in swarms shapes (Pinel-Alloul 1995). Overall smaller scales (0.1 to 10 m), individual behaviours and responses can override physical processes (Zhou *et al*. 1994).

Not all potential swarm shapes may be viable and the associated swarm shape parameters may be constrained within certain limits. Across different scales, the relationships between these parameters may follow geometric rules and some level of predictability in observed swarm shape may be apparent. Identifying these scaling rules has value in understanding the mechanisms of swarm formation (and break-up) since they can reveal patterns of assembly that are followed by individuals when joining (or leaving) an aggregation. Furthermore, the interaction between size and shape has wider implications to ecosystem function, particularly with regards a biomass dominant species such as Antarctic krill. The horizontal and vertical extent of swarms may influence their relative availability to different predator types, so differentially affecting foraging success (Croxall *et al*. 1999, Brierley and Cox 2015). For instance, horizontally extensive swarms may benefit aerial predators whereas vertically extended swarms may be more exclusively available to diving predators. The biogeochemical role of swarms may also be affected by the relationship between size

and shape, particularly in the ability of swarms to flux faecal pellet carbon to the ocean interior, which can be accelerated when swarms are vertically extensive (Tarling and Thorpe 2017).

Krill are believed to aggregate actively mainly through social interactions (Weber *et al*. 1986). These interactions, in turn, are likely to be influenced by physiological factors, such as hunger and hypoxia, and external conditions, such as the presence of predators, food availability and ambient temperature. Individual krill within swarms are able to behave collectively to their mutual benefit, for instance, in allowing them to retain favourable feeding locations (Tarling and Thorpe 2014) or to obtain some physiological advantage (Swadling *et al*. 2005, Ritz *et al*. 2001). How these drivers translate to internal swarm structure is nevertheless complex and only limited insights have so far been gained. Kawaguchi *et al*. (2010) found that shoals of krill in captivity had nearest neighbour distances of around 2-3 body lengths. Catton *et al* (2011) found krill to be aligned so that they were out of the downward wake of neighbours, as predicted from flow analysis on individuals by Wiese (1996).

At the whole swarm level, ultimate swarm shape may be further influenced by both the positive and negative consequences of group living. There is general consensus that swarming benefits its members by reducing predation risk through lowered predator encounter rate, collective vigilance, rapid information transfer and predator confusion (Ritz *et al*. 2011). Nevertheless, if predation were the only influence, then the optimal swarm shape should be spherical because this combines the smallest surface for any volume, minimising both the risk of discovery and the numbers of individuals at the swarm edge (Brierley and Cox 2010, Hemelrijk and Hildenbrandt 2012). That this is clearly not the case for the majority of swarms indicates that there are other antagonistic influences on swarm shape. One of the main costs of swarm membership is reduced feeding rates from exploitative and interference mechanisms (Folt 1987). Furthermore, the reduced levels of diffusion may lead to waste products concentrating in the swarm interior to the point where they become toxic (Ritz *et al*. 2011) and oxygen saturation drops to levels that are physiologically limiting (Johnson

78 *et al*. 1984). Such costs place a pressure on the swarm to disperse, so allowing greater diffusion and
79 reducing the distance of individuals to the swarm edge. Ultimate swarm shape therefore reflects
80 both the costs and the benefits of swarming.

81 A further influential factor on swarm shape is the scale of the swarm. Smaller swarms may not
82 be under the same physical and biological influences as larger ones. For instance, levels of
83 interference between individuals and diffusive flux to the swarm interior may be markedly different
84 between small and large swarms. Conditions within the swarm must also remain within tolerable
85 limits for individual swarm members if the swarm is to remain viable. These factors could mean that
86 changes in swarm size are accompanied by changes in shape that follow certain allometric rules. This
87 in turn will constrain the relationship between swarm shape parameters.

88 In this study, we examine a large dataset of krill swarms visualised acoustically during a scientific
89 survey of the southwest Atlantic sector of the Southern Ocean. Our working hypothesis is that
90 swarm shape, considered in terms of parameters such as area, perimeter, length and vertical
91 thickness, conforms to geometric scaling functions that limit their variability. We will test this
92 hypothesis through considering scaling laws between various geometrical parameters and defining
93 the ranges of their variability.

94 Our analysis considers data collected in 2-dimensions through what are 3–dimensional objects,
95 meaning that our insights into the true size and dimensions of any one individual swarm are limited.
96 Nevertheless, the advantage of our dataset is that it consists of swarm cross-sections collected along
97 preset transects, meaning that the direction passed through each individual swarm is random. Over
98 a large number of swarms, the fact that each observation is random allows us to build up a picture of
99 what patterns are common and what geometric relationships are statistically significant. We do not
100 resolve the temporal evolution of swarm formation or break up of any one swarm but rather obtain
101 an instantaneous picture of thousands of swarms within which we expect different states, or types,
102 to exist. The insights we gain into geometric constraint on krill swarms are important in helping to

identify the controlling influences on krill swarming behaviour. They are also useful when considering ecosystem structure, such as predator-prey dynamics and foraging on prey patches as well as the influence of different swarm formations on the flow of carbon through the system.

Methods

General survey details. A survey encompassing 8 transects was carried out by the RRS *James Clark Ross* across the Scotia Sea between 9 January and 16 February 2003 (Fig. 1A). The majority of transects were transited at 10 knots, although it was necessary to slow to around 5 knots in a small number of regions where conditions were icy. Acoustic data were collected using a SIMRAD EK60 echosounder connected to hull-mounted split-beam 38 kHz, 120 kHz and 200 kHz transducers. Only data from the 38 kHz and 120 kHz transducers were analysed to identify krill swarms to a maximum depth of 300 m. The beam angles, and hence sampling volumes, of both these frequencies were the same (7°) so allowing direct comparisons to be made for the purposes of swarm identification across most depths. An offset of the two sounders means that the beams were not overlapping at depths shallower than 25 m. Although this could lead to the misidentification of some krill swarms, we worked on the assumption that swarms of that shape, size, and backscattering strength were unlikely to be anything other than Antarctic krill in this part of the Southern Ocean. The surveys encompassed both open-ocean and shelf regions, but all shelf data (data < 100 km from nearest land) were excluded from the present analysis since swarms adopt very different formations in shelf environments and can be considered a special case worthy of separate investigation (Klevjer *et al*. 2010). Data were collected continuously and subsequent analyses included both daytime and nighttime periods.

Krill net sampling. A number of swarms were captured by net sampling to ground-truth the acoustic records, principally for the purpose of establishing an acoustic target strength for krill. Krill swarms were located using the Simrad echosounder and then sampled with a rectangular midwater trawl (RMT8). The RMT8 was rigged with two remotely operated opening/closing nets, which had the capacity to sample separate swarms in close vicinity to one another. Krill sampling took place mostly during the hours of darkness. Full details of this analysis are provided in Tarling *et al*. (2009).

Acoustic data and processing. An acoustic system calibration was undertaken at Stromness Bay (54°9.44'S, 36°41.99'W) on 17 February 2003 using the standard sphere method (Foote *et al.*, 1987, 1990). Calibration was carried out with a 60 mm copper sphere for the 38 kHz transducers and a 23 mm copper sphere for the 120 kHz transducers (Tarling *et al.,* 2009).

Raw acoustic data from the 38 kHz and 120 kHz transducers were processed using Sonardata Echoview version 4.0 following the protocol of Hewitt *et al.,* (2004) with the aim of excluding all backscatter not attributable to krill aggregations. Background noise was estimated and subtracted from the 38 kHz and 120 kHz echograms (Watkins & Brierley, 1996), assuming that background noise levels follow a $20\log R + 2\alpha R$ relationship (where R is depth and α is the attenuation coefficient), which is then scaled to the minimum volume backscatter (S_v) in each layer during a transect before subtracting from the respective echograms. This method is particularly effective at decreasing the distortion with depth that would otherwise occur when identifying targets with a dB differencing approach (see below). Filters were applied to exclude the upper 13 m of the water column and depths below the detected bottom (where applicable) and other "bad data" resulting from interference or stormy weather. Smaller spikes were removed from the data by restricting the final swarm detection to those regions of the echogram where the 7 × 7 (pings × samples where the ping interval was 1.5 s and sample length, 0.1867 m) convolution filtered data were above a threshold of –80 dB at 120 kHz. A threshold of –70 dB at 120 kHz was used in the subsequent swarm delineation, as advised by Lawson *et al.,* (2008).

Krill swarm delineation. A swarm detection algorithm was applied to the processed 120 kHz echogram data using Sonardata Echoview version 4.0 "School detection module" (Sonardata Pty, Tasmania, Australia), which employs a SHAPES algorithm (Coetzee, 2000). This algorithm identifies data points that can be determined as "swarm candidates", which are groups of cells that meet minimum criteria for length and thickness. These individual swarm candidates are then linked together to form a larger swarm candidate if the horizontal and vertical distances between them are less than the specified maximum linking distances. After all linking has been carried out, swarms are

recognised if the final swarm candidates are larger than the defined minimum total swarm length and thickness. With a ping interval of 1.5 s, and standard cruising speed of 10 knots, the minimum horizontal resolution was around 7.5 m. We set the minimum total swarm length to 15 m, which is double the minimum horizontal resolution. Transmit pulse duration was 1024 µs, giving an approximate pulse length of 1.5 m and a minimum vertical distance between 2 resolved targets of ~75 cm. Minimum swarm candidate length and thickness were set to 10 m and 1 m, respectively. The maximum horizontal linking distance was set to 15 m, following Woodd-Walker *et al.,* (2003), and the maximum vertical linking distance was set to 5 m. Swarms where the relative school length image compared to the beam width (Nb_i) was less than 1.5 were excluded from the dataset, following Diner (2001).

Swarms were detected from the 120 kHz echograms, and physical and acoustic descriptors for the detected swarm-regions were exported from both 38 and 120 kHz data. These dimensions were corrected for known beam geometry according to the system of Diner (1998) within Sonardata Echoview 4.0. Detected swarms were interrogated to determine whether or not they were krill using the variable $\Delta S_{v120\text{-}38}$ identification technique (CCAMLR, 2005) following the steps outlined in Tarling *et al.,* (2009), including the allocation of different krill total lengths to different survey regions in line with corresponding net catch results. This had a relatively minor influence on estimated krill target strength (TS) across the survey grid (Tarling *et al* 2018).

Swarm descriptors. Directions passed through swarms were random in that a swarm cross-section represents the transit across a swarm as the ship follows its preset route (Fig. 1B). Once scaled according to distance travelled, we calculated a number of geometrical properties for each swarm cross-section: (i) P, the perimeter (m), (ii) A, the area of this section (m^2), (iii) L, the maximal horizontal extent (m) and (iv) T_{max}, maximal vertical extent (m). T_{max} represents the range between the uppermost and lowermost part of the swarm, which captures the fact that some parts of a swarm are located higher or lower in the water column than others. An alternative measure is the mean thickness averaged along swarm length, which can be defined as (v) $T_{mean} = A/L$. This

parameter defines the average distance between the upper and lower borders of a swarm and is always smaller than T_{max}. For convenience, we also denote the logarithm of swarm thickness as $\tau = \log_{10} T$.

Numerical analysis. We investigated relationships between swarm descriptors through regression based analyses. All regressions were carried out in the logarithmic domain with the Matlab routine fitln using the relationship $\log y = b + k\log x$. In most cases, the results were later converted into a more convenient power law form, $y = 10^b x^k$.

Results

Scaling of length and thickness. There was a wide range of swarms sizes detected in the survey, with swarm length varying from 1 m to 10,000 m, maximal thickness from 1 m to 100 m, and the average thickness from 0.3 m to 10 m. To give an insight into swarm size distributions, consider the bivariate histograms showing the distribution of swarms in (L, T_{max}) coordinates and (L, T_{mean}) coordinates (Figs. 2A and B).

The distribution of swarm thicknesses shifts towards greater values as swarm length increases. To take into account the dependence of the distribution parameters on swarm length, we fit them for each length bin separately. The histogram of logarithmic thickness (both maximal, T_{max}, and average, T_{mean}) in each length bin can be closely approximated by a normal distribution truncated at the minimum detection limit for swarm thickness of 1.27 m (Fig. S1)

$$P_L(\tau) \propto \exp\left(-\frac{(\tau-\tau^*(L))^2}{2\sigma^2(L)}\right)\theta(\tau-\tau_{min}) \qquad (1)$$

where both the mean $\tau^*(L)$ and variance $\sigma^2(L)$ depend on swarm length, $\theta(\tau-\tau_{min})$ is the Heaviside function, and τ_{min} is the logarithmic thickness of the thinnest detected swarm (see Appendix A for the fitting details). A Shapiro-Wilk test confirmed the normality of these distributions at the significance level $\alpha = 0.01$ for swarms longer than $L > 30$ m. The obtained maximal likelihood estimates for $\tau^*(L)$ and $\sigma(L)$ with error bars indicating 95% confidence interval are shown in Fig. 2.

The most likely logarithmic maximal thickness τ^*_{max} (Fig. 2A) and average thickness τ^*_{mean} (Fig. 2B) monotonically increase with swarm length. While τ^*_{max} increases proportionally to the logarithm of length over the entire range, the average thickness τ^*_{mean} remains approximately constant (around 1 m) for swarms shorter than 40 m and begins to increase with L for longer swarms. The

linear regression analysis (Table 1) shows that the most likely maximal thickness increases as $\tau^*_{max}(L) = -0.62 + 0.69\log_{10} L$ (Fig. 2A) and its standard deviation decreases as $\sigma(L) = 0.51 - 0.11\log_{10} L$ (Fig. 2A). For the average thickness, we obtain $\tau^*_{mean} = 0.058$ ($T^*_{mean} = 1.14$ m) for $L < 40$ and $\tau^*_{mean} = 0.69 + 0.47\log_{10} L$ for $L \geq 40$ m and $\sigma = 0.39 - 0.05\log_{10} L$. Thus, both maximal and average thickness increase slower than swarm length. For instance, for $L \geq 40$m, the average thickness increases approximately as a square root of length, $T^*_{mean} = 4.9L^{0.47} \approx 4.9\sqrt{L}$, meaning that a two order of magnitude increase in swarm length (e.g., from 40m to 4000 m) leads only to approximately one order of magnitude increase in the average thickness (from 27 m to 240 m for the given example).

Scaling of swarms in the vertical realm. We obtain an additional perspective on the scaling of swarm shape from the distribution of T_{max}/T_{mean}, which is the relative vertical maximum swarm extent with respect to mean thickness. This parameter can be interpreted as swarm flatness, as it increases when the vertical swarm variation increases without increasing the mean thickness, and it approaches 1 for an absolutely flat swarm with no variation along the vertical axis. Swarm flatness first increases with length from 2 for $L = 10$ m to 5 for $L \approx 400$m and then stays at a constant level or even decreases for extremely long swarms with the average value of $\langle T_{max}/T_{mean} \rangle \approx 4.8$ in this range (Fig. 2C).

The swarm aspect ratio, T_{max}/L, decreases with swarm length (Fig. 3A). Aspect ratio is greatest in the smallest swarms but declines dramatically as swarms increase in length. Using the dependence of the most likely maximal thickness on the length to estimate the aspect ratio we obtain:

$$\frac{T^*_{max}}{L} = 0.26L^{-0.32} \quad (2)$$

i.e., the aspect ratio decreases approximately inversely proportional to the cubic root of L. As shown in Fig. 3A, this equation provides a good approximation to the linear regression through the data points. For example, whereas 10 m long swarms exhibit an aspect ratio of around 1 m of thickness per 5 m for length, 1000 m long swarms have proportions of 1 m of thickness per 30 m or more of length.

Scaling of perimeter to area. Swarm area and perimeter can be approximated by a power function of length and maximal thickness (Fig. 4). The swarm area scales as $A = 0.8L^{0.77}T_{max}$ and perimeter as $P = 3.5L^{0.86}T_{max}^{0.48}$. Both functions describe 95% of the variance in swarm area and perimeter.

The scaling of swarm area allows us to make some conclusions concerning the scaling of the average swarm thickness. Using the scaling expression for area, we can calculate the average thickness as $T_{mean} = A/L = 0.8\,T_{max}L^{-0.23}$ m. Thus, on average, the mean swarm thickness is smaller than the maximal thickness T_{max} by the factor $0.8L^{-0.23}$.

The area specific length of perimeter, surface roughness $R = P/A$ on average equals 3.17 m^{-1}. Using the scaling laws for area and perimeter, we find:

$$R = \frac{P}{A} = 4.36\,L^{0.09}T_{max}^{-0.52}\,m^{-1} \quad (3)$$

Thus, surface roughness has an extremely weak dependence on length and mainly depends on swarm maximal thickness. Indeed, the factor $L^{0.09}$ changes from 1 for $L = 1\text{m}$ to 2.29 for $L = 10\,000$ m. Thus, the main variations in the surface roughness are related to the changes in thickness. Using median value $L_{median} = 41$ m, we obtain the following approximate equation for swarm roughness:

$$R_{appox} = 4.36\, L_{median}^{0.09} T_{max}^{-0.52} = 6.16 T_{max}^{-0.52}\ \mathrm{m}^{-1} \quad (4)$$

Hence, surface roughness is approximately inversely proportional to the square root of swarm thickness. Eq. (4) closely approximates a linear regression of data points (Fig. 3B).

It is not surprising that surface roughness decreases with swarm size because perimeter typically grows slower than area with increasing size. It is more informative, therefore, to compare surface roughness with roughness of a smooth geometrical figure with the same linear dimensions. For this purpose, we calculate surface roughness of ellipses with the same length and thickness (Fig. 3B). As shown in Appendix B, and confirmed by linear regression of the data, the roughness of an ellipse decreases approximately as $1/T_{max}$, which is much faster than the decrease of surface roughness we observe in krill swarms ($1/T_{max}^{0.46}$). Increasing swarm size appears to be accompanied by the appearance of new cavities and indentations in the swarm structure which leads to an increase in the perimeter. As a result, the perimeter of thick swarms can be up to 10 times greater than the perimeter of an ellipse with the same linear dimensions.

Swarm categorisations. To address the hypothesis that swarm size constrains swarm shapes to certain types, we compare the area and perimeter of swarms with that of dimensionally equivalent ellipses. We denote the relative elongation in swarm perimeter with respect to ellipse perimeter as $\varepsilon_P = P/P_{ell}$ and ratio of swarm to ellipse area as $\varepsilon_A = A/A_{ell}$. For most of swarms, ε_P is greater than 1 and ε_A is less than 1. Only in extremely rare situations, e.g. when the swarm shape approaches to, for instance, a rectangular or rhombus, are these rules violated (see frequencies of swarms with different values of ε_P and ε_A in Fig. 5B). The greatest concentration of swarms is around the median values $\varepsilon_P^* = 1.9$ and $\varepsilon_A^* = 0.4$. Thus the most frequent swarms are approximately 2 times greater in perimeter and 2 times smaller in area than the corresponding ellipse. However, these swarms

represent less than 10% of the total swarm number because most of the swarms are distributed within the peripheral areas of the plot.

Using the median values as thresholds, we split swarms into the following four equally abundant classes (Fig. 5A) with distinctly different geometrical properties. (I) *Ellipsoidal* swarms: perimeter and area are close to the perimeter and area of an ellipse - these swarms are the most compact and their shape approaches to an ellipse. (II) *Filamentous* swarms: the area approximately equals the area of an ellipse, but the perimeter is larger due to filaments and fjords in the swarm structure - these swarms are still compact apart from at the edges; (III) *Needle-like* swarms: the perimeter approximately equals the ellipse perimeter, but the area is smaller - these swarms are thin and elongated with a small number of cavities. (IV) *Indented* swarms: the area is smaller than the area of the corresponding ellipse, but the perimeter is greater - these swarms have the largest perimeter and smallest area, and therefore, the highest surface roughness for given linear dimensions.

How does the swarm class depend on swarm linear dimensions? To answer this question, consider the change in ε_P and ε_A with swarm maximal thickness and length (Fig. 6). Although the pattern is relatively noisy, we observe clear gradients with the perimeter ratio ε_P increasing mainly with swarm thickness and area ratio ε_A decreasing with swarm length. The dashed lines show the isolines where the averaged values of ε_P and ε_A equal the threshold levels ε_P^* and ε_A^* (see also Supplementary Fig. S2). Superpositioning of the threshold levels gives us the swarm class partitioning in (L,T_{max}) axes and shows what types and sizes of swarms are geometrically compatible (Fig. 6C).

Our comparison of the swarm and ellipse surface roughness (Fig. 3B) shows that roughness of geometrical shapes typically decreases with shape size. This fact hampers a direct comparison of the roughness of differently sized swarms and produces a false sense that larger swarms should be smoother whilst, in reality, larger swarms possess a more complex perimeter structure. Generalizing our approach further, we define the relative swarm roughness as $\rho = R_{swarm}/R_{ellipse}$, where $R_{ellipse}$

308 is the roughness of an ellipse with the same linear dimensions. It is easy to check that the relative
309 roughness can be also expressed in terms of the relative perimeter and area as $\rho = \varepsilon_P/\varepsilon_A$.
310 Combining the estimations of the average swarm roughness, Eq. 3, with ellipse roughness (Appendix
311 B) we find that the average relative roughness scales as

312 $$\rho = 1.72\, L^{0.09}\, T_{max}^{0.48} \quad (5)$$

313 Thus, the relative surface roughness depends mainly on the changes in the vertical swarm extent,
314 increasing approximately as the square root of T_{max}, and is nearly independent of the swarm length.

Discussion

Through examining a large dataset of acoustically visualised krill swarms in the southwest Atlantic sector of the Southern Ocean, we identified that the shapes adopted by swarms varied according to their size. We uphold our working hypothesis that the influence of geometric constraints is strong on relationships between swarm parameters such as area, perimeter, length, vertical thickness and swarm shape. Not all swarm shapes appeared possible at all scales, and whereas swarms could be smooth and vertically thick at smaller scales, larger scale swarms either exhibited relative thinning or increased numbers of indentations and filaments. We discuss further the nature of these geometric relationships and consider potential environmental and physiological factors that may influence them.

Scaling of length and thickness. We found that swarms were more likely to lengthen than to increase in vertical thickness as the scale of the swarm increases. The effect is most exaggerated in the largest swarms because thickness grows approximately as the square root of length and a two order of magnitude increase in length (e.g. from 40 m to 400 m) results in only a one order of magnitude increase in thickness (from 27 m to 240 m in the given example). From the perspective of swarm shape, therefore, an increase in swarm size is mostly observed as an increase in length and not thickness. This is also observed when deriving a scaling of the aspect ratio (T/L) which we found to decrease as the power of swarm length. Whereas 10 m long swarms exhibit an aspect ratio of around 0.2 (1 m thickness per 5 m length), 1000 m long swarms have a ratio of 0.03 (1 m of thickness per 30 m or more of length), indicating that increases in length are not accompanied by proportional increases in thickness.

Aspect ratio was also considered in Antarctic krill swarms found in Crystal Sound and Marguerite Bay as well as Laubeuf fjord by Zhou and Dorland (2004). They found that aspect ratio in the Crystal Sound and Marguerite Bay population differed considerably from that in the Laubeuf Sound population, with the former tending towards a ratio of 0.05 and the latter, 0.01 to 0.03. This was

attributed to lateral stretching by the greater levels of advection in Laubeuf Sound. Furthermore, swarms in Laubeuf Sound were longer than those in Crystal Sound and Marguerite Bay, which would also contribute to the general decrease in aspect ratio, as we found in the present study.

The tendency for swarms to lengthen but not thicken vertically with increasing swarm size may also be influenced by individual swimming behaviour and inter-individual relationships. Antarctic krill swims through the metachronal beating of its abdominal appendages (pleopods) which, unlike fish, does not involve any undulation of the body. Comparatively, this means that they do not require as much lateral space on either side to swim without interference. Packing concentrations of krill in Scuba and laboratory observations are notably high, with minimal nearest neighbour distances of between 1.5 and 3 body lengths being reported (O'Brien 1989, Kawaguchi *et al*. 2010, Catton *et al*. 2011). Collectively, krill generate considerable downdrafts (Kils 1981, Catton *et al*. 2011, Tarling and Thorpe 2017), which are necessary to overcome their negative buoyancy (Kils 1981). From an individual perspective, it is less energetically expensive for krill to join others through swimming in front of, behind or to the side of existing swarm members rather than to join from above or below. In terms of small aggregations, avoidance of any collective downdrafts below the swarm would also make joining another swarm laterally less costly energetically than from beneath. Scaled up to the level of the swarm therefore, adding to the length rather than the vertical thickness of a swarm appears to be a more energetically efficient strategy, which is consistent with our observations.

Scaling of swarms in the vertical realm. We distinguished between two measures of vertical swarm thickness, T_{max}, which represents the maximum distance between the upper and lower extremities of a swarm, and T_{mean}, which is the mean vertical thickness across the entire length of a swarm. We found that the average T_{max} monotonically increased as a power of swarm length, faster than the average T_{mean}, which stayed approximately constant at around 1m for swarms shorter than 50 m and only then began to increase. The ratio of T_{max} to T_{mean} increased for swarms shorter than 400 m length and levelled off at around 5 for longer swarms. The fact that T_{mean} always remained about

366 1/5th of T_{max} in larger swarms indicates that external swarm shape remains relatively conservative
367 with regards the relationship between vertical extremities and the main body of the swarm.

368 Both biological and physical factors may limit the T_{mean} and T_{max} of large swarms. Biologically, the
369 euphotic zones reaches it maximum depth between 50 and 80 m in the Scotia Sea (Korb *et al*. 2012),
370 such that primary production is unlikely to occur below such depths. Thus, deeper than 100 m, krill
371 may have limited possibilities to feed on fresh phytoplankton. Nevertheless, Tarling and Thorpe
372 (2017) demonstrated that individuals are likely to move vertically within the body of a swarm and
373 rotate through the main phytoplankton layers as they repeatedly feed and sink. This behaviour has
374 also been observed in mysids (Buskey 1998). The behaviour allows individuals within vertically thick
375 swarms access to the food layers, at least for a period of time. Maximum vertical thickness may
376 accordingly represent the distance over which individuals sink after feeding before returning to the
377 upper layers to feed once again. This sinking behaviour may also influence the relatively fixed
378 relationship between the T_{max} and T_{mean} in larger swarms.

379 The structure of the water column may also present vertical limits to swarm coherence. In summer,
380 the upper mixed layer reaches a maximum depth of around 100 m in the Scotia Sea (Venables *et al*.
381 2012), below which is colder Winter Water (Gordon *et al*. 1977). The pycnocline at the bottom of the
382 mixed layer may be a physical barrier to further vertical expansion of a swarm. Furthermore, the
383 strength and direction of currents in the upper mixed layer and the Winter Water may differ
384 (Murphy *et al*. 2004), potentially presenting a shear that may challenge the ability of deeper
385 individuals to remain with the rest of the swarm.

386 **Scaling of perimeter to area.** The perimeter of an object will always decrease relative to its area if
387 the object increases in size while retaining the same shape. We calculated this effect for ellipses with
388 the same dimensions and showed that if $L \gg T_{max}$ (which is a valid assumption for most swarms),
389 the perimeter to area ratio (surface roughness) should decrease as $1/T_{max}$ (see Appendix B).
390 However, for krill swarms with increasing T_{max}, we found that surface roughness in krill swarms

391 decreases less steeply and can be approximated as the inverse square root of T_{max}. This means that
392 the perimeter of krill swarms grow with swarm length faster than compared to the perimeter of an
393 ellipse. To highlight this effect, we introduced the relative roughness parameter, ρ, as the ratio of
394 swarm roughness to ellipse roughness. This value increases approximately as the square root of the
395 swarm maximal thickness and has only a weak positive dependence on swarm length. This measure
396 of swarm roughness is more consistent with an intuitive expectation of what should happen when
397 two swarms merge. For instance, joining two similar swarms in the same horizontal layer may
398 double the swarm length but should have only a weak effect on the swarm thickness and perimeter
399 structure. This is reflected in the weak dependence of the relative roughness on swarm length. By
400 contrast, a vertical merging of two swarms can double the swarm thickness and lead to a more
401 complex and rougher perimeter structure with a larger number of cavities and filaments. We
402 observe an increase of the relative swarm roughness with increasing thickness.

403 In their analysis of the three dimensional structure of Antarctic krill swarms using a multibeam sonar
404 in inshore locations, Brierley and Cox (2010) found that swarm size and packing density varied
405 greatly but surface area:volume (3D surface roughness) ratios were distributed around a fixed value
406 of 3.3 m^{-1}. This is not entirely consistent with our own observations of surface roughness, albeit with
407 our 2 dimensional rather than 3-dimensional perspective, since we found that surface roughness
408 decreases with increasing swarm size. Nevertheless, we agree with the findings of Brierley and Cox
409 (2010) in two regards, firstly in the mean perimeter:area ratio being approximately the same as the
410 surface area:volume ratio (3.2 m^{-1} versus 3.3 m^{-1} respectively) and, secondly, that with increasing
411 swarm size, surface area (or perimeter in the present case) decreased less in relation to area than it
412 would for an equivalent isometrically scaled object. The three-dimensional visualisations provided by
413 Brierley and Cox (2010) provides an unrivalled insight into swarm structure although their krill
414 surveys were more spatially limited and likely encountered a comparatively smaller spectrum of
415 swarm types than those considered in the present study. In the future, it would be instructive to
416 carry out intercomparisons of two- and three dimensional visualisations from data collected

simultaneously to consider how respective geometric relationships (e.g. surface area to volume versus perimeter to area) relate to each other. The wider use of lower-frequency sonar would be particularly useful in this regard (Makris *et al*. 2006).

Further influences on geometric relationships. Variance around geometric relationships likely results from both internal and external factors. Internally, packing concentrations will influence the external smoothness of swarms. Tighter packing will be generated from the polarisation of individuals, which potentially is a response to predator avoidance or a product of directional horizontal migrations (Hamner & Hamner 2000). Predator avoidance behaviour may be particularly acute in shelf regions close to higher predator colonies which may be responsible for the considerably different swarming patterns observed in such regions (Klevjer *et al*. 2010). Looser packing is generated from more individualistic behaviour, as would result from filter feeding when encountering a patch of phytoplankton (Kawaguchi *et al*. 2010). Externally, day-night differences are likely to be a major source of variance. Tarling *et al*. (2018) found that levels of dissimilarity between certain swarm parameters altered according time of day with, for instance, area and perimeter exhibiting a significant linkage in similarity during the daytime, but no linkage during dusk and nighttime. The authors concluded that swarm parameters were more variable than depth over the diel cycle. Distinguishing the individual contributions of these factors to variance in geometric relationships is nevertheless far from straightforward given that there will also be inter-relationships between the factors themselves e.g. individualistic behaviour from feeding is more likely to occur during dusk and nighttime.

Swarm categorisations. Based on the relationship between perimeter and area, we classified krill swarms into four shape types, which we termed *Ellipsoidal*, *Filamentous, Needle-Like* and *Indented*. Certain features of the different swarm types suggest the influence of different behaviours. For instance, swarm types with lower than average perimeters (*Ellipsoidal* and *Needle-like*) are most compact and retain a relatively smooth periphery, which may reflect that individuals within these

swarms are tightly aggregated. At a behavioural level, this could be generated through krill being in a phase of active horizontal migration, where nearest neighbour distances are reduced and relative positions become polarised in order to gain maximal hydrodynamic benefit (Wiese 1996, Catton *et al*. 2011). Reduction of the perimeter may also be a response to predators such that the largest possible proportion of individuals occupy internal sheltered positions away from the edge (Brierley and Cox 2010).

Indented swarms have above average perimeter but below average area and are more amorphous in shape. The shape likely reflects that packing concentrations are not uniformly high, resulting in large indents in the external shape of swarms and possibly even vacuoles within the body of the swarm. Such features have also been identified in fish schools (Rieucau *et al*. 2015, Freon *et al*. 1992), taken to indicate that individuals were exhibiting more individualistic or exploratory behaviour in low stress situations with greater inter-individual distances and lower polarisation. This would be consistent with krill swarms that are exploiting patches of food, particularly in terms of using their feeding baskets to filter food particles where greater inter-individual distances would be required (Hamner 1984, O'Brien 1988).

Filamentous swarms may also be a product of more individualistic behaviour although their above average areas indicate that a larger proportion of individuals are some distance away from the swarm nucleus. This suggest some heterogeneity in the tendencies of individuals with only local groups reaching out from the swarm edge to form filaments (Parrish and Edelstein-Keshet 1999). These local groups may have different physiological states to the larger majority, necessitating greater levels of feeding. For instance, in Northern krill, Tarling (2003) found that females were prepared to take greater levels of risk compared to males and sub-adults to meet a greater energetic demand. Individuals about to moult or mate may also displace themselves from the body of the swarm to avoid cannablism of themselves or their offspring, respectively (Tarling *et al*. 1999). The

466 filaments may otherwise reflect a stage prior to the break-up of a swarm, akin to the "stretch and
467 tear" phases of fish schools described by Freon *et al*. (1992).

468 Besides different behavioural constraints, swarm shape type is also constrained by swarm
469 size. Thin swarms are mostly either *Ellipsoidal* (when short) or *Needle-like* (when long). By contrast,
470 most thick swarms are characterised by a complex perimeter and are either *Filamentous* (when
471 short) or *Indented* (when long). This relationship occurs because the relative swarm area and
472 perimeter strongly depend on swarm thickness and length. An increase of swarm thickness increases
473 mainly the relative perimeter ε_P but not relative area ε_A, which can be associated with an increased
474 amount of filaments and indentations at the swarm edge. By contrast, increasing swarm length
475 reduces swarm relative area but not perimeter. In particular, the area of short swarms,
476 independently of their thickness, is close to the area of an ellipse with the same dimensions but the
477 area of long swarms tends to be nearly one order of magnitude smaller than the area of an ellipse.
478 Thus, indentation and relative thinning appear to be a necessary feature for long swarms to remain
479 coherent.

480 **Influence of swarm shape and size on ecosystem function.** Knowledge of the spectrum of shapes
481 and sizes of swarms have a utility to considering how ecosystems are structured. For Southern
482 Ocean ecosystems in particular, interactions between higher predators and their krill prey has a
483 dominating influence on how the system functions (Murphy *et al*. 2007). Different predators have
484 widely varying methods of foraging. The ways in which they exploit food patches are an important
485 aspect of their life-cycle, shaping their response to varying levels of prey availability (Croxall *et al*.
486 1999). Here we illustrate that horizontally extensive krill swarms are unlikely to be also vertically
487 extensive. This may therefore differentially favour aerial foragers who have the ability to locate rare
488 but large patches and exploit them from surface layers (Grünbaum and Veit 2003). Diving predators,
489 by contrast, may benefit more from exploiting smaller swarms, which are more likely to be thicker
490 relative to their length and more exclusively available to predators that can forage deeper for their

prey (Croxall *et al*. 1985). Our parameterisations can be used to recreate prey fields in models to test these hypotheses (e.g. Cresswell *et al*. 2007).

Antarctic krill are also increasingly recognised as a major conduit for carbon export to the ocean interior through large scale deposition of sinking faecal pellets (Belcher *et al*. 2017). Not all swarms may be equally as efficient in this process, and swarm shape may be a major determinant of export efficiency. Vertically extensive swarms are likely to release faecal pellets towards the bottom of the mixed layer (Tarling and Thorpe 2017), while pellets released by long and thin swarms may have further to travel before reaching the ocean interior, increasing their chance of interception and remineralisation by coprophagous species. We provide a means of accounting for the types and characteristics of different swarm shapes that may assist in the determination of carbon export efficiency by krill.

Concluding remarks. We identified rules that govern the comparative external dimensions of open ocean krill swarms. We identify clear geometric relationships between swarm parameters and uphold the hypothesis that swarm shape is bound by geometric functions across scales. These rules are likely to reflect a combination of physical and biological influences that are external to the swarm and behavioural interactions between individuals within the swarm itself. As swarms increase in size, they tend to lengthen horizontally far more than thicken vertically and this likely reflects both biological and physical constraints placed on swarm dimensions. We also identified characteristic relationships between the perimeter and area of swarms, variance in which may reflect different stages in the time course of swarms, particularly phases of feeding and horizontal migration. Certain shapes may also indicate heterogeneity between swarm members with regards physiological state. Although the shapes of krill swarms are highly variable, we demonstrate that there is some predictability in their dimensions. These findings will have utility both to considering the size and shape of food patches for krill predators and in accounting for the biogeochemical role of different swarms types.

Acknowledgements

We thank the contribution of the two anonymous referees whose insights and suggestions greatly improved this manuscript. We are grateful to the crew and scientists aboard the RRS James Clark Ross during the cruise JR82 for their assistance in collecting material. We also thank D. Bone for assembling and maintaining the net gear and N. Cunningham for organising and retrieving data. S. Fielding and T. Klevjer assisted in the acoustic identification and visualization of krill swarms, as reported in previously published works. ABR acknowledges the Lower Saxony Ministry for Science and Culture, project POSER. GT acknowledges COMICS (UK Natural Environment Research Council Large grant NE/M020762/1) in supporting the write up of this manuscript. The work was carried out as part of the Ecosystems programme at the British Antarctic Survey and Natural Environment Research Council.

References

Belcher, A., Tarling, G., Manno, C., Atkinson, A., Ward, P., Skaret, G., Fielding, S., *et al*. 2017. The potential role of Antarctic krill faecal pellets in efficient carbon export at the marginal ice zone of the South Orkney Islands in spring. Polar Biology, 40: 2001-2013.

Brierley, A. S., and Cox, M. J. 2010. Shapes of krill swarms and fish schools emerge as aggregation members avoid predators and access oxygen. Current Biology, 20: 1758-1762.

Brierley, A. S., and Cox, M. J. 2015. Fewer but not smaller schools in declining fish and krill populations. Current Biology, 25: 75-79.

Buskey, E. J. 1998. Energetic cost of position-holding behavior in the planktonic mysid *Mysidium columbiae*. Marine Ecology Progress Series, 172: 139-147.

Catton, K. B., Webster, D. R., Kawaguchi, S., and Yen, J. 2011. The hydrodynamic disturbances of two species of krill: implications for aggregation structure. Journal of Experimental Biology, 214: 1845-1856.

CCAMLR 2005. Report of the first meeting of the subgroup on acoustic survey and analysis methods SC-CCAMLR-XXIV/BG/3.

Coetzee, J. 2000. Use of a shoal analysis and patch estimation system (SHAPES) to characterize sardine schools. Aquatic Living Resources, 13: 1-10.

Cresswell, K. A., Tarling, G. A., and Trathan, P. N. 2007. Weight loss during breeding is adaptive for female macaroni penguins, *Eudyptes chrysolophus*. Evolutionary Ecology Research, 9: 1053-1076.

Croxall, J. P., Everson, I., Kooyman, G. L., Ricketts, C., and Davis, R. W. 1985. Fur-seal diving behavior in relation to vertical distribution of krill. Journal of Animal Ecology, 54: 1-8.

Croxall, J. P., Reid, K., and Prince, P. A. 1999. Diet, provisioning and productivity responses of marine predators to differences in availability of Antarctic krill. Marine Ecology Progress Series, 177: 115-131.

Diner, N. 1998. Correction on school geometry and density: approach based on acoustic image

554 simulation. ICES Conference and Meeting Documents, B:1: pp. 51.
555 Diner, N. 2001. Correction on school geometry and density: approach based on acoustic image
556 simulation. Aquatic Living Resources, 14: 211-222.
557 Folt, C. 1987. An experimental analysis of costs and benefits of zooplankton aggregation. *In*
558 Predation, Direct and Indirect Impacts on Aquatic Communities, pp. 300-314. Ed. by J.
559 Benndorf. University Press of New England, Hanover and London. 386 pp.
560 Folt, C. L., and Burns, C. W. 1999. Biological drivers of zooplankton patchiness. Trends in Ecology &
561 Evolution, 14: 300-305.
562 Foote, K. G., Everson, I., Watkins, J. L., and Bone, D. G. 1990. Target strength of Antarctic krill
563 (*Euphausia superba*) at 38 and 120 kHz. Journal of the Acoustic Society of America, 87: 16-
564 24.
565 Foote, K. G., Knudsen, F. R., Vestnes, G., MacLennan, D. N., and Simmonds, E. J. 1987. Calibration of
566 acoustic instruments for fish density estimation: a practical guide. ICES Cooperative
567 Research Report, 144: pp. 69.
568 Fréon, P., Gerlotto, F., and Soria, M. 1992. Changes in school structure according to external stimuli:
569 description and influence on acoustic assessment. Fisheries Research, 15: 45-66.
570 Gordon, A. L., Georgi, D. T., and Taylor, H. W. 1977. Antarctic polar frontal zone in the western Scotia
571 sea - summer 1975. Journal of Physical Oceanography, 7: 309-328.
572 Grünbaum, D., and Veit, R. R. 2003. Black-browed albatrosses foraging on Antarctic krill: density-
573 dependence through local enhancement? Ecology, 84: 3265-3275.
574 Hamner, W. M. 1984. Aspects of schooling of *Euphausia superba*. Journal of Crustacean Biology, 4
575 (Special Issue): 67-74.
576 Hamner, W. M., and Hamner, P. P. 2000. Behavior of Antarctic krill (*Euphausia superba*): schooling,
577 foraging, and antipredatory behavior. Canadian Journal of Fisheries and Aquatic Sciences,
578 57: 192-202.
579 Hemelrijk, C. K., and Hildenbrandt, H. 2012. Schools of fish and flocks of birds: their shape and

internal structure by self-organization. Interface focus: rsfs20120025.

Hewitt, R. P., Watkins, J., Naganobu, M., Sushin, V., Brierley, A. S., Demer, D., Kasatkina, S., *et al*. 2004. Biomass of Antarctic krill in the Scotia Sea in January/February 2000 and its use in revising an estimate of precautionary yield. Deep-Sea Research Part II: Topical Studies in Oceanography, 51: 1215-1236.

Johnson, M. A., Macaulay, M. C., and Biggs, D. C. 1984. Respiration and excretion within a mass aggregation of *Euphausia superba*: Implications for krill distribution. Journal of Crustacean Biology, 4: 174-184.

Kawaguchi, S., King, R., Meijers, R., Osborn, J. E., Swadling, K. M., Ritz, D. A., and Nicol, S. 2010. An experimental aquarium for observing the schooling behaviour of Antarctic krill (*Euphausia superba*). Deep-Sea Research Part II: Topical Studies in Oceanography, 57: 683-692.

Kils, U. 1981. Swimming behaviour, swimming performance and energy balance of Antarctic krill *Euphausia superba*. BIOMASS Scientific Series, 3: pp. 1-121.

Klevjer, T. A., Tarling, G. A., and Fielding, S. 2010. Swarm characteristics of Antarctic krill *Euphausia superba* relative to the proximity of land during summer in the Scotia Sea. Marine Ecology Progress Series, 409: 157-170.

Korb, R. E., Whitehouse, M. J., Ward, P., Gordon, M., Venables, H. J., and Poulton, A. J. 2012. Regional and seasonal differences in microplankton biomass, productivity, and structure across the Scotia Sea: Implications for the export of biogenic carbon. Deep-Sea Research Part II: Topical Studies in Oceanography, 59: 67-77.

Krafft, B. A., Skaret, G., Knutsen, T., Melle, W., Klevjer, T., and Soiland, H. 2012. Antarctic krill swarm characteristics in the Southeast Atlantic sector of the Southern Ocean. Marine Ecology Progress Series, 465: 69-83.

Lawson, G. L., Wiebe, P. H., Stanton, T. K., and Ashjian, C. J. 2008. Euphausiid distribution along the Western Antarctic Peninsula - Part A: Development of robust multi-frequency acoustic techniques to identify euphausiid aggregations and quantify euphausiid size, abundance and

606 biomass. Deep-Sea Research Part II: Topical Studies in Oceanography, 55: 412-431.
607 Makris, N. C., Ratilal, P., Symonds, D. T., Jagannathan, S., Lee, S., and Nero, R. W. 2006. Fish
608 population and behavior revealed by instantaneous continental shelf-scale imaging. Science,
609 311: 660-663.
610 Murphy, E. J., Thorpe, S. E., Watkins, J. L., and Hewitt, R. 2004. Modeling the krill transport pathways
611 in the Scotia Sea: spatial and environmental connections generating the seasonal
612 distribution of krill. Deep-Sea Research Part II: Topical Studies in Oceanography, 51: 1435-
613 1456.
614 Murphy, E. J., Watkins, J. L., Trathan, P. N., Reid, K., Meredith, M. P., Thorpe, S. E., Johnston, N. M.,
615 *et al*. 2007. Spatial and temporal operation of the Scotia Sea ecosystem: a review of large-
616 scale links in a krill centred food web. Philosophical Transactions of the Royal Society B-
617 Biological Sciences, 362: 113-148.
618 O'Brien, D. P. 1988. Surface schooling behavior of the coastal krill *Nyctiphanes australis* (Crustacea,
619 Euphausiacea) off Tasmania, Australia. Marine Ecology Progress Series, 42: 219-233.
620 O'Brien, D. P. 1989. Analysis of the internal arrangement of individuals within crustacean
621 aggregations (Euphausiacea, Mysidacea). Journal of Experimental Marine Biology and
622 Ecology, 128: 1-30.
623 Parrish, J. K., and Edelstein-Keshet, L. 1999. Complexity, pattern and evolutionary trade-offs in
624 animal aggregation. Science, 284: 99-101.
625 Pinel-Alloul, P. 1995. Spatial heterogeneity as a multiscale characteristic of zooplankton community.
626 Hydrobiologia, 300: 17-42.
627 Rieucau, G., Fernö, A., Ioannou, C. C., and Handegard, N. O. 2015. Towards of a firmer explanation of
628 large shoal formation, maintenance and collective reactions in marine fish. Reviews in Fish
629 Biology and Fisheries, 25: 21-37.
630 Ritz, D. A., Foster, E. G., and Swadling, K. M. 2001. Benefits of swarming: mysids in larger swarms
631 save energy. Journal of the Marine Biological Association of the United Kingdom, 81: 543-

544.

Ritz, D. A., Hobday, A. J., Montgomery, J. C., and Ward, A. J. W. 2011. Social aggregation in the pelagic zone with special reference to fish and invertebrates. *In* Advances in Marine Biology vol. 60, pp. 161-227. Ed. by M. Lesser. Elsevier, Amsterdam. 272 pp.

Schmidt, K., and Atkinson, A. 2016. Feeding and food processing in Antarctic krill (*Euphausia superba* Dana). *In* Biology and Ecology of Antarctic Krill, pp. 175-224. Ed. by V. Siegel. Springer, Switzerland. 441 pp.

Siegel, V., and Kalinowski, J. 1994. Krill demography and small-scale processes: a review. *In* Southern Ocean ecology: the BIOMASS perspective, pp. 145-164. Ed. by S. Z. El-Sayed. Cambridge University Press, Cambridge, England. 446 pp.

Swadling, K. M., Ritz, D. A., Nicol, S., Osborn, J. E., and Gurney, L. J. 2005. Respiration rate and cost of swimming for Antarctic krill, *Euphausia superba*, in large groups in the laboratory. Marine Biology, 146: 1169-1175.

Tarling, G. A. 2003. Sex-dependent diel vertical migration in northern krill *Meganyctiphanes norvegica* and its consequences for population dynamics. Marine Ecology Progress Series, 260: 173-188.

Tarling, G. A., Cuzin-Roudy, J., and Buchholz, F. 1999. Vertical migration behaviour in the northern krill *Meganyctiphanes norvegica* is influenced by moult and reproductive processes. Marine Ecology Progress Series, 190: 253-262.

Tarling, G. A., Klevjer, T., Fielding, S., Watkins, J. L., Atkinson, A., Murphy, E., Korb, R., *et al*. 2009. Variability and predictability of Antarctic krill swarm structure. Deep-Sea Research Part I: Oceanographic Research Papers, 56: 1994–2012.

Tarling, G. A., and Thorpe, S. E. 2014. Instantaneous movement of krill swarms in the Antarctic Circumpolar Current. Limnology and Oceanography, 59: 872-886.

Tarling, G. A., and Thorpe, S. E. 2017. Oceanic swarms of Antarctic krill perform satiation sinking. Proceedings of the Royal Society B, 284: 20172015.

658 Tarling, G. A., Thorpe, S. E., Fielding, S., Klevjer, T., Ryabov, A., and Somerfield, P. J. 2018. Varying
659 depth and swarm dimensions of open-ocean Antarctic krill *Euphausia superba* Dana, 1850
660 (Euphausiacea) over diel cycles. Journal of Crustacean Biology, 38: 716-727.
661 Venables, H., Meredith, M. P., Atkinson, A., and Ward, P. 2012. Fronts and habitat zones in the Scotia
662 Sea. Deep-Sea Research Part II: Topical Studies in Oceanography, 59: 14-24.
663 Watkins, J. L., and Brierley, A. S. 1996. A post-processing technique to remove background noise
664 from echo integration data. Ices Journal of Marine Science, 53: 339-344.
665 Weber, L. H., El-Sayed, S. Z., and Hampton, I. 1986. The variance spectra of phytoplankton, krill and
666 water temperature in the Antarctic Ocean, south of Africa. Deep Sea Research Part A:
667 Oceanographic Research Papers, 33: 1327-1343.
668 Wiese, K. 1996. Sensory capacities of euphausiids in the context of schooling. Marine and
669 Freshwater Behaviour and Physiology, 28: 183-194.
670 Woodd-Walker, R. S., Watkins, J. L., and Brierley, A. S. 2003. Identification of Southern Ocean
671 acoustic targets using aggregation, backscatter and shape characteristics. Ices Journal of
672 Marine Science, 60: 641-649.
673 Zhou, M., and Dorland, R. D. 2004. Aggregation and vertical migration behavior of *Euphausia*
674 *superba*. Deep-Sea Research Part II: Topical Studies in Oceanography, 51: 2119-2137.
675 Zhou, M., Nordhausen, W., and Huntley, M. 1994. ADCP measurements of the distribution and
676 abundance of euphausiids near the Antarctic Peninsula in winter. Deep-Sea Research Part I:
677 Oceanographic Research Papers, 41: 1425-1445.

678 ## Figures

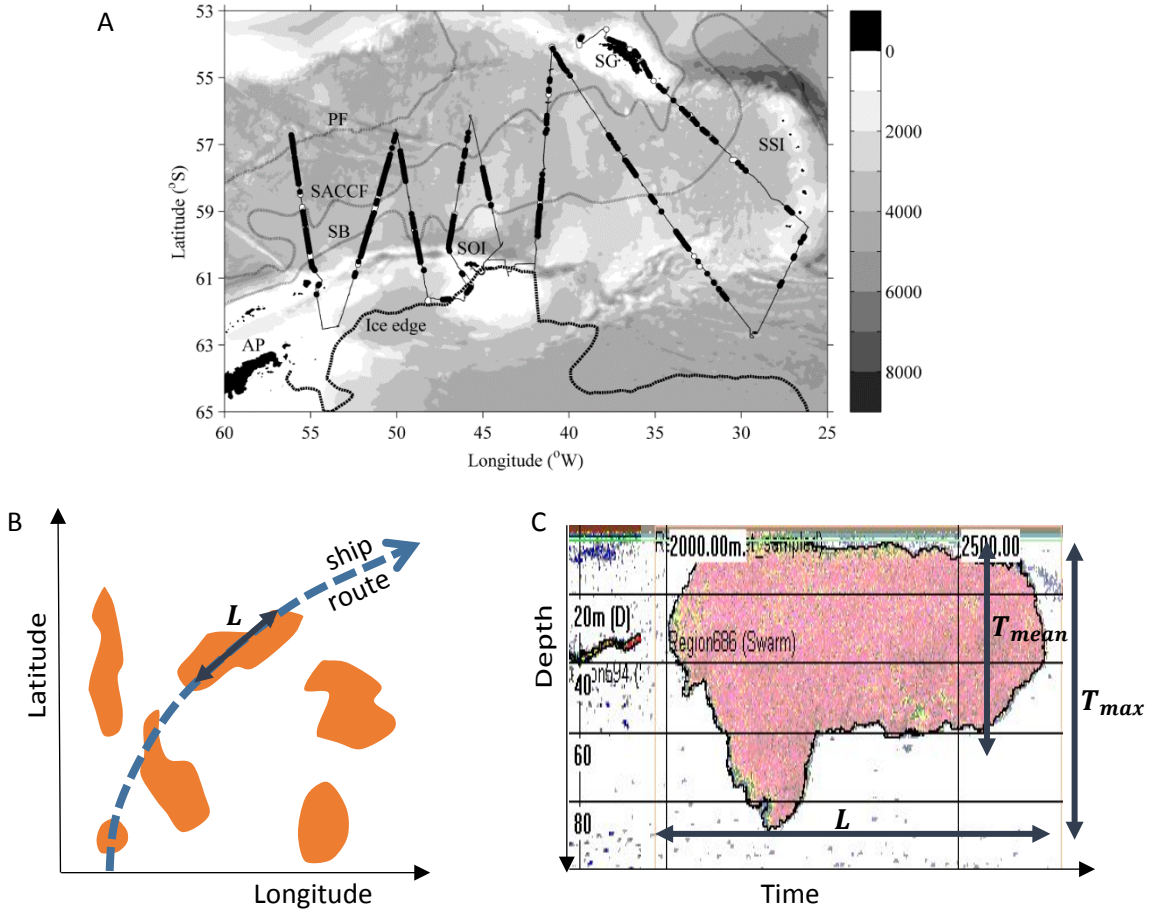

679

680 Fig. 1: **Swarms of Antarctic krill**. **(A)** The ship route in the Atlantic sector of the Southern Ocean
681 during the survey in 2003 highlighting in black circles the location of intercepted krill swarms. **(B)** A
682 schematic representation of a ship route with respect to krill swarms (view from above). The ship
683 route can intersect krill swarms at various angles. **(C)** Sampled echogram of a krill swarm obtained
684 along the ship route (side view). The measured parameters: swarm length L is the maximal linear
685 extent of the swarm along the ship route; maximal thickness T_{max} is the distance between the
686 uppermost and downmost parts of the swarm; area A is the filled area within the swarm; perimeter
687 P is the total linear distance around the swarm edge. Additionally, we calculate the mean thickness
688 as $T_{mean} = A/L$.

689

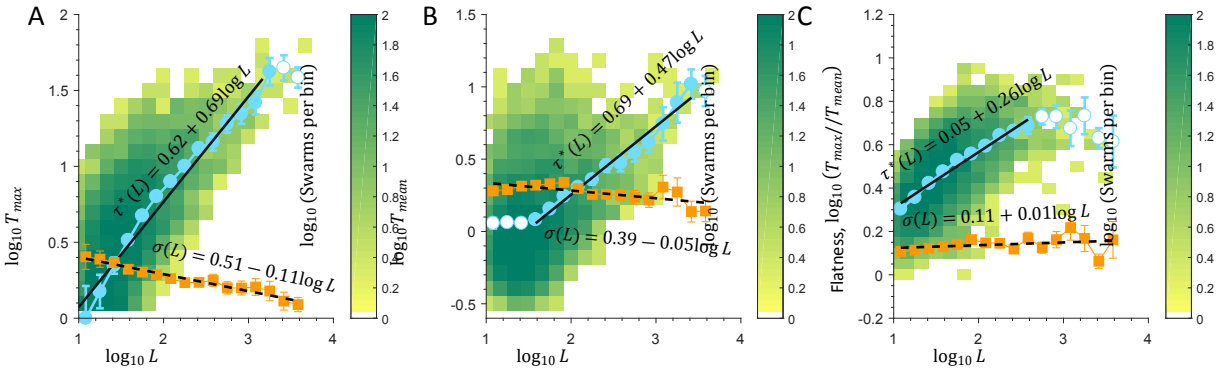

690

691 Fig. 2: **Length and thickness distribution of krill swarms in the south-west Atlantic sector**.

692 Bivariate swarm distribution (colour coded) of logarithms of swarm length (horizontal axis) vs. **(A)**

693 maximal thickness, T_{max}, **(B)** mean thickness, T_{mean}, and **(C)** flatness, T_{max}/T_{mean} (vertical axes).

694 The grid is logarithmically binned with step 1/6 for $\log_{10} L$ and 0.1 for vertical axes. Within each

695 length class (vertical grid columns), the distribution closely follows a normal distribution truncated at

696 the detection limit, $T_{min} = 1.27$ m (see Fig. S1 for some examples). The maximal likelihood estimates

697 for the parameters of the distribution: most likely logarithmic thickness $\tau^*(L)$ (open and closed

698 blue circles) and variance $\sigma(L)$ (orange circles), the error bars show standard error. The linear

699 regression (excluding outlier points marked as blue open circles) of the mean values (black solid line)

700 and the variance (black dashed line). See Table 1 for the regression parameters.

701

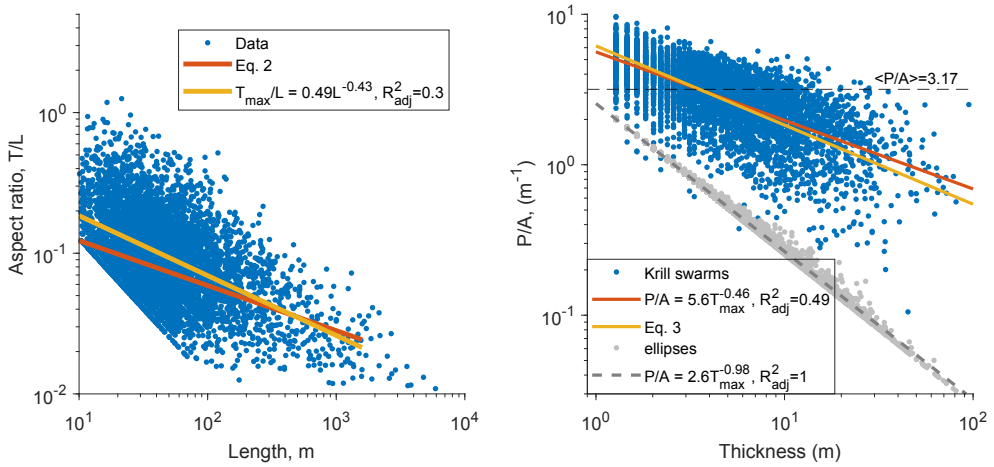

703

704 Fig. 3: **Scaling of swarm aspect ratio and surface roughness. (A)** Aspect ratio (Thickness/Length)

705 of krill swarms as a function of length (blue dots), linear regression of data (yellow line) in

706 comparison with an approximation provided by Eq. 2 (red line). **(B)** Surface roughness

707 (Perimeter/Area) of krill swarms as a function of swarm thickness (blue dots) compared to the

708 surface roughness of ellipses with the same linear dimensions (grey dots) with the average level of

709 3.17 m^{-1} (black dashed line). Linear regression of surface roughness of krill swarms (red line) in

710 comparison with an approximation provided by Eq. 3 (yellow line). Linear regression of the surface

711 roughness of ellipses (grey dashed line).

712

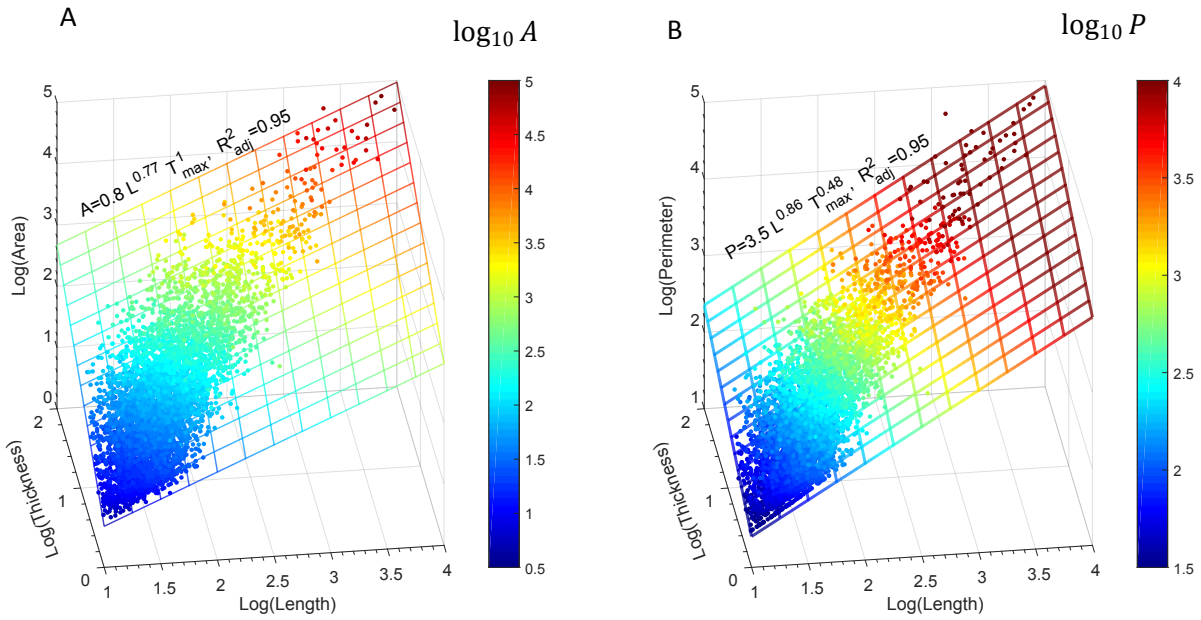

713

714 Fig. 4: **Scaling rules for swarm area (A) and perimeter (B)**. Swarm area and perimeters (dots)

715 fitted with planes (grid lines) in log-log space. The colour coding of the grid lines on the planes and

716 data points matches the vertical coordinates ($\log_{10} A$ and $\log_{10} P$) to highlight the closeness of data

717 points and fitted planes. Both fittings explain 95% of variance in the data.

718

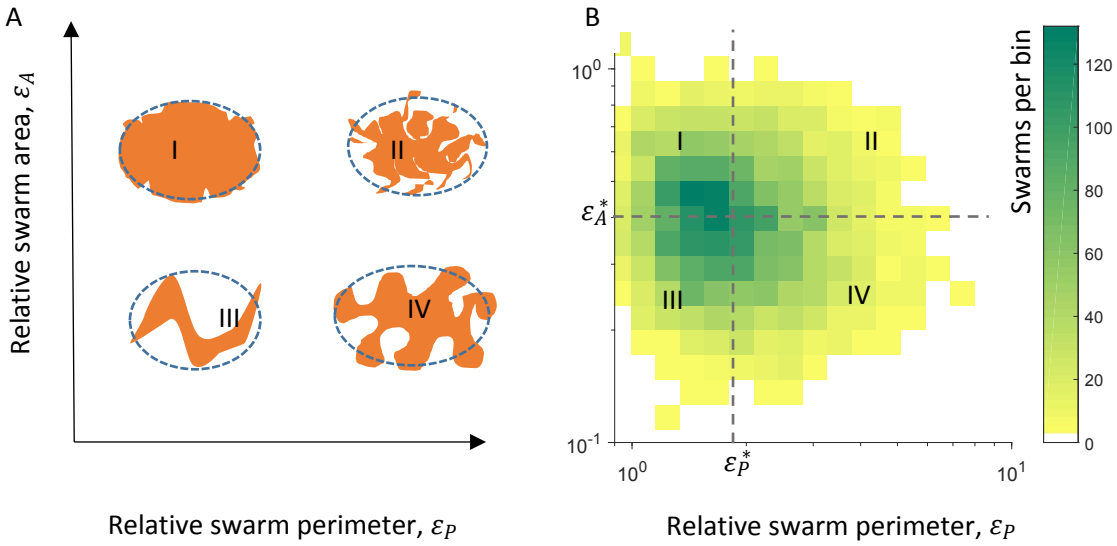

719

720 Fig. 5: **Classification of krill swarms. (A)** A schematic representation of different classes of
721 swarm shapes. The shape of swarms (orange) is compared to an ellipse (blue dashed line) with the
722 same linear dimensions. As coordinates, we use the relative swarm area, ε_A, and relative perimeter,
723 ε_P, with respect to the area and perimeter of the corresponding ellipse. We introduce the following
724 classes (I) *Ellipsoidal* swarms: perimeter and area are close to the perimeter and area of an ellipse.
725 (II) *Filamentous* swarms: the area approximately equals to the ellipse area, but the perimeter is
726 larger. (III) *Needle-like* swarms: The perimeter is approximately equal to the ellipse perimeter, but
727 the area is smaller than the ellipse area. (IV) *Indented* swarms. The area is smaller than the area of
728 an ellipse, but the perimeter is greater than the ellipse perimeter. **(B)** The bivariate plot of swarm
729 distribution as a function of relative swarm area, ε_A, and relative perimeter, ε_P. The number of
730 swarms as a function of the relative area and perimeter (logarithmically binned, colour coded). The
731 border between different classes (dashed lines).

732

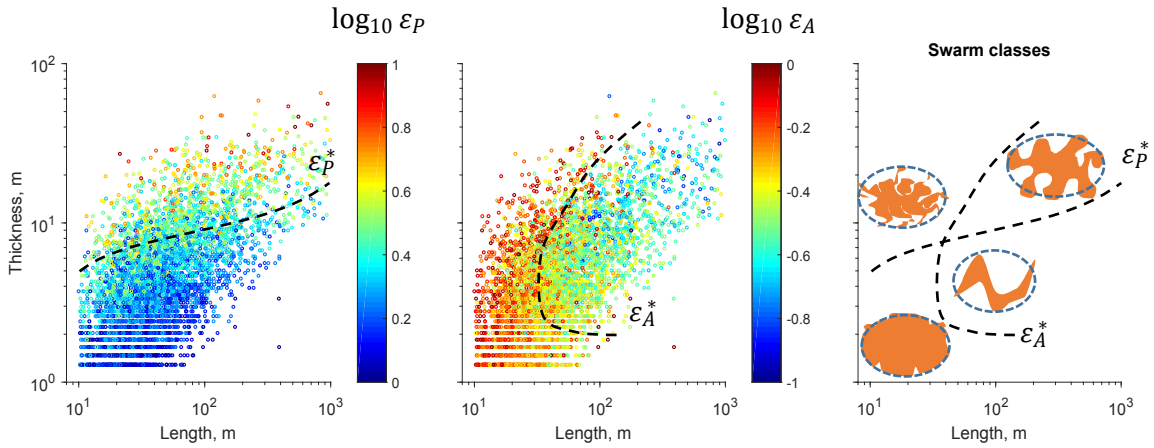

733

734 Fig. 6: **Swarm classification as a function of length and thickness. (A)** Swarm relative perimeter

735 ε_P (colour coded) as a function of swarm length and maximal thickness. **(B)** The same but for swarm

736 relative area ε_A. **(C)** Location of the swarm classes in (L, T_{max}) coordinates. Threshold levels ε_P^* and

737 ε_A^* (black dashed lines).

738 ## Tables

739 Table 1. Linear regression parameters for $\tau^* = b + k\log_{10} L$ and $\sigma(L) = b + k\log_{10} L$ for Fig.

740 2.

	$b \pm$ Stand err	$k \pm$ Stand err	R^2_{adj}
Fig. 2A			
$\tau^*_{max}(L)$	-0.62±0.07	0.69±0.03	0.98
$\sigma(L)$	0.51±0.02	-0.112±0.007	0.95
Fig. 2B			
$\tau^*_{mean}(L)$	-0.69±0.07	0.47±0.03	0.97
$\sigma(L)$	0.39±0.03	-0.05±0.01	0.47
Fig. 2C			
$\tau^*(L)$	0.05±0.02	0.26±0.01	0.98
$\sigma(L)$	0.11±0.03	0.01±0.01	0.02

741

Appendix A. Truncated Gaussian distribution

Typically fitting a Gaussian distribution requires finding the mean and variance of the data. This approach gives a correct result only if the data distribution is symmetrical and the mean value coincides with the most likely value where the Gaussian distribution reaches a maximum. If the data is truncated (as for instance in Fig. S1A), then this algorithm does not work, as the mean value will lie in the middle of the histogram and will be greater than the most likely value. To determine the parameters correctly in this case we need to fit a truncated Gaussian distribution defined only on the range where the data is available. This function can be defined as

$$P_L(\tau) = \frac{\theta(\tau - \tau_{min})}{\mathrm{erf}\left(-\tau_{min}, -\tau^*, \sigma\right)} e^{-\frac{(\tau - \tau^*(L))^2}{2\sigma^2(L)}} \qquad (eqS1)$$

where $\theta(\tau - \tau_{min}) = \begin{bmatrix} 0, & \tau \le \tau_{min} \\ 1, & \tau > \tau_{min} \end{bmatrix}$ is the Heaviside function and the normalizing factor is given by the normal cumulative distribution function

$$\mathrm{erf}\left(-\tau_{min}, -\tau^*, \sigma\right) = \frac{1}{\sigma\sqrt{2\pi}} \int_{\tau_{min}}^{\infty} e^{-\frac{(\tau - tau^*)^2}{2\sigma^2}}$$

To fit this distribution we used the function fitdist_ntrunc (https://mathworks.com/matlabcentral/fileexchange/64040-fitting-a-truncated-normal-gaussian-distribution).

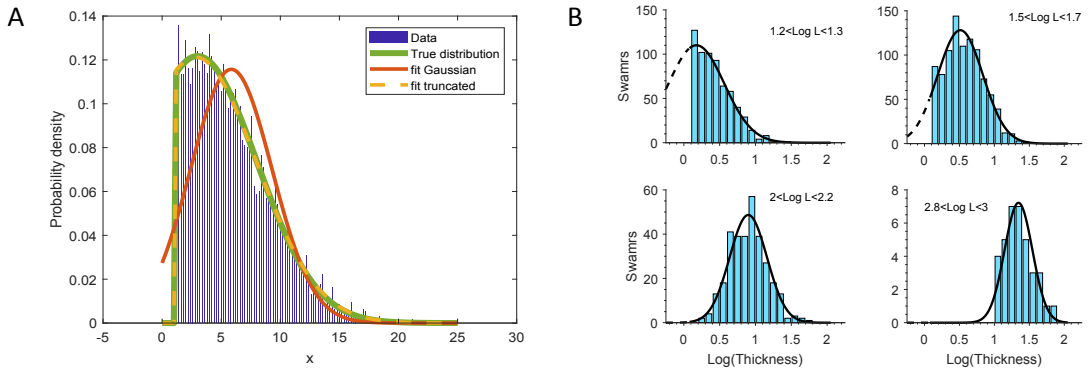

Fig. S1: **Fitting truncated density distribution. (A)** Comparison of the probability density functions fitted to normally distributed random values truncated at $x = 1$. Histogram of data points (blue bars) drawn from a truncated Gaussian distribution (green line). Fitting a simple Gaussian distribution to the histogram results in a function shifted to the right (red line) because the mean value of the truncated distribution does not coincide with the peak of the distribution. By contrast, fitting a truncated Gaussian distribution (yellow dashed line) provides a correct result that matches the initial distribution function. **(B)** Sample histograms of logarithm of maximal thickness for different length classes fitted with a truncated normal distribution (solid line in the range where data is available and dashed in the truncated range).

Appendix B. Surface roughness of an ellipse

The area of an ellipse with the semi-axes $a = L/2$ and $b = T_{max}/2$ equals

$$A_{ell} = \pi L T_{max}/4$$

The ellipse perimeter can be approximately calculated using Ramanujan formula

$$P_{ell} = \pi\left(\frac{3L}{2} + \frac{3T_{max}}{2} - \sqrt{\left(\frac{3L}{2} + \frac{T_{max}}{2}\right)\left(\frac{L}{2} + \frac{3T_{max}}{2}\right)}\right)$$

Calculating their ratio under the assumption that $L \gg T_{max}$ (which happens when L is large) we find

$$R_{ell} = \frac{P_{ell}}{A_{ell}} = \frac{2(3-\sqrt{3})}{T_{max}} = \frac{2.54}{T_{max}}$$

The obtained analytical formula is very close the linear regression result $R_{ell} = \frac{10^{0.41}}{T_{max}^{0.98}} = \frac{2.57}{T_{max}^{0.98}}$ (Fig. 3B, grey dashed line).

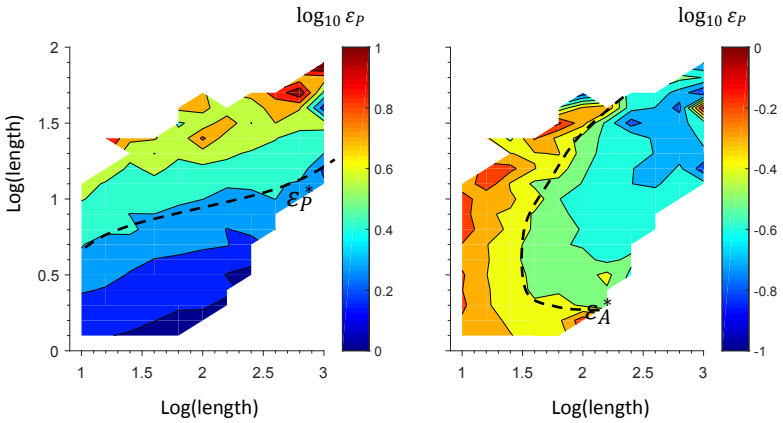

36

37 Fig. S2: Average level of the shape factors ε_P and ε_A as a function of swarm length and thickness

38 (colour coded). The isolines where the average values equal the median values ε_P^* and ε_A^* (black

39 dashed lines).

40

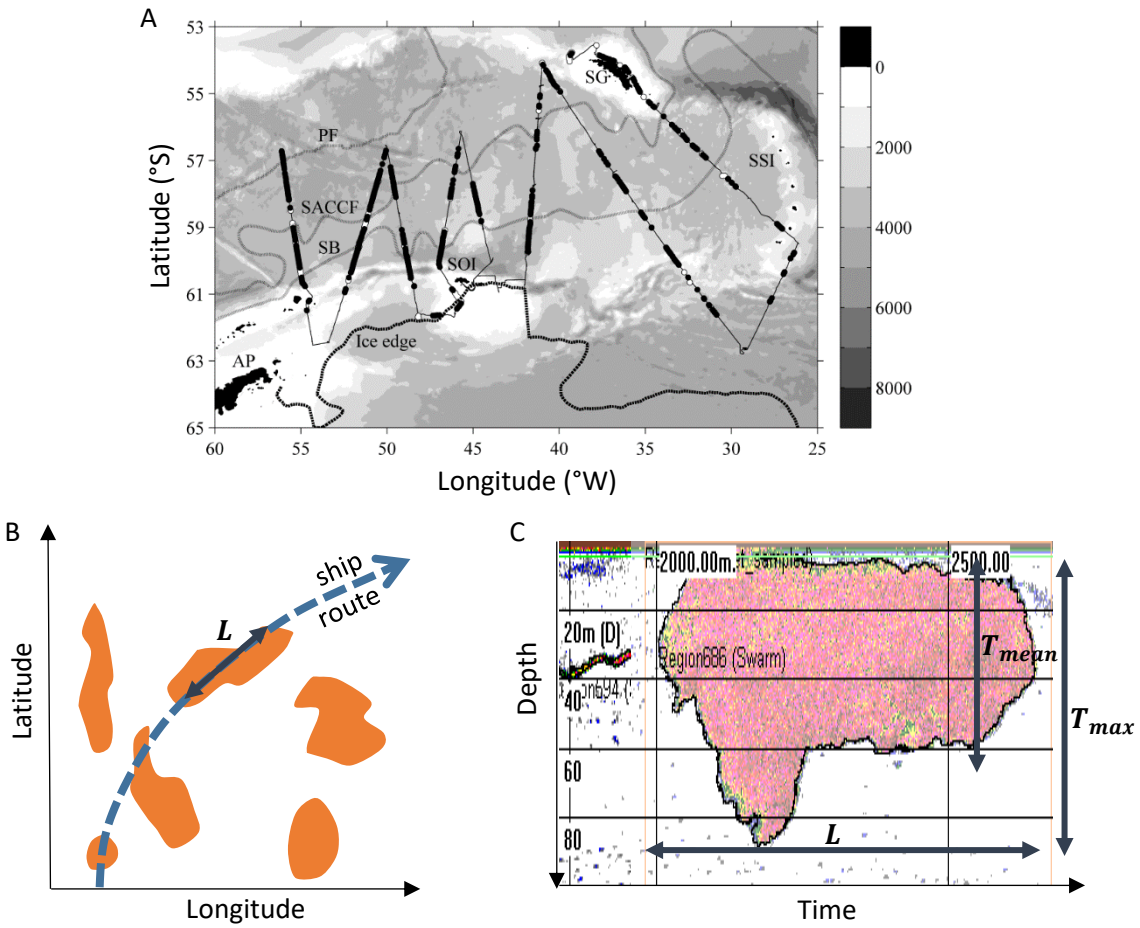
A
Latitude (°S)
Longitude (°W)
PF
SACCF
SB
SOI
SG
SSI
Ice edge
AP
0
2000
4000
6000
8000
B
Latitude
Longitude
ship
route
L
C
Depth
Time
2000.00m
2500.00
20m (D)
Region686 (Swarm)
T_{mean}
T_{max}
L

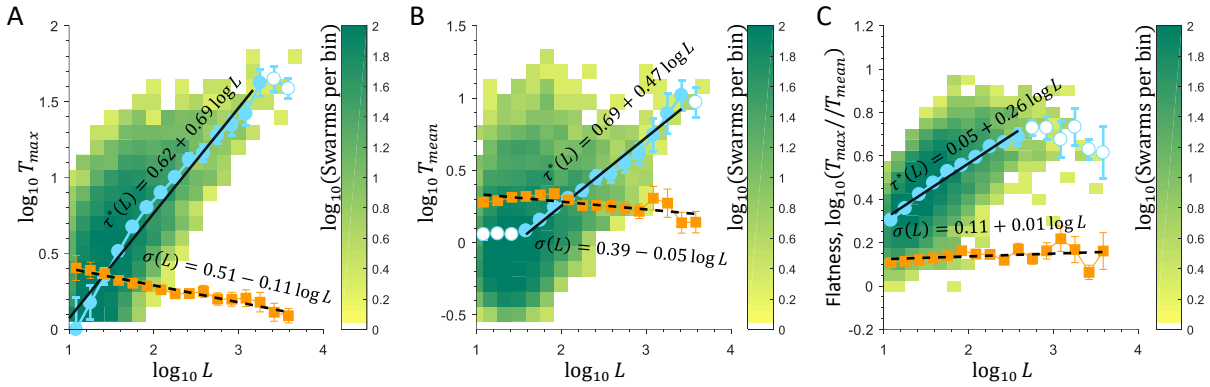
A
B
C
$\log_{10} T_{max}$
$\log_{10} T_{mean}$
Flatness, $\log_{10}(T_{max}/T_{mean})$
$\log_{10} L$
$\log_{10}$(Swarms per bin)
$\tau^*(L) = 0.62 + 0.69 \log L$
$\sigma(L) = 0.51 - 0.11 \log L$
$\tau^*(L) = 0.69 + 0.47 \log L$
$\sigma(L) = 0.39 - 0.05 \log L$
$\tau^*(L) = 0.05 + 0.26 \log L$
$\sigma(L) = 0.11 + 0.01 \log L$

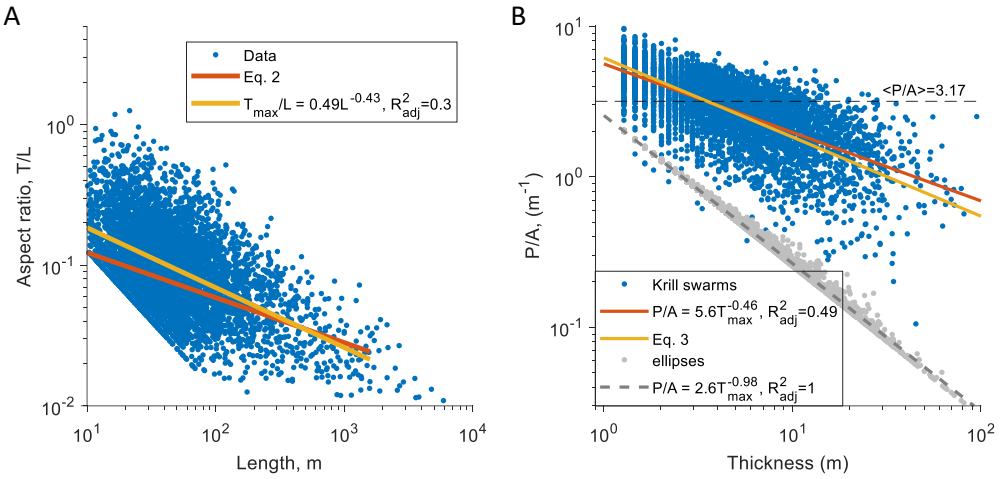
A
Data
Eq. 2
$T_{max}/L = 0.49L^{-0.43}$, R^2_{adj}=0.3
Aspect ratio, T/L
Length, m
B
<P/A>=3.17
Krill swarms
$P/A = 5.6T_{max}^{-0.46}$, R^2_{adj}=0.49
Eq. 3
ellipses
$P/A = 2.6T_{max}^{-0.98}$, R^2_{adj}=1
P/A, (m^{-1})
Thickness (m)

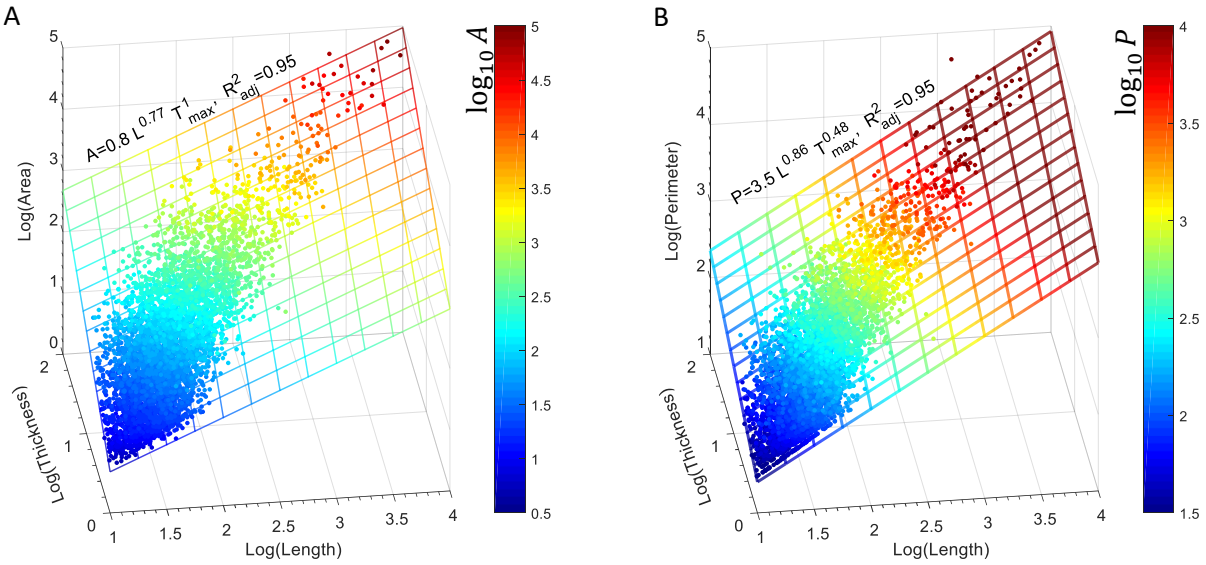
A
A=0.8 L^0.77 T^1_max, R^2_adj=0.95
Log(Area)
Log(Thickness)
Log(Length)
log10 A
B
P=3.5 L^0.86 T^0.48_max, R^2_adj=0.95
Log(Perimeter)
Log(Thickness)
Log(Length)
log10 P

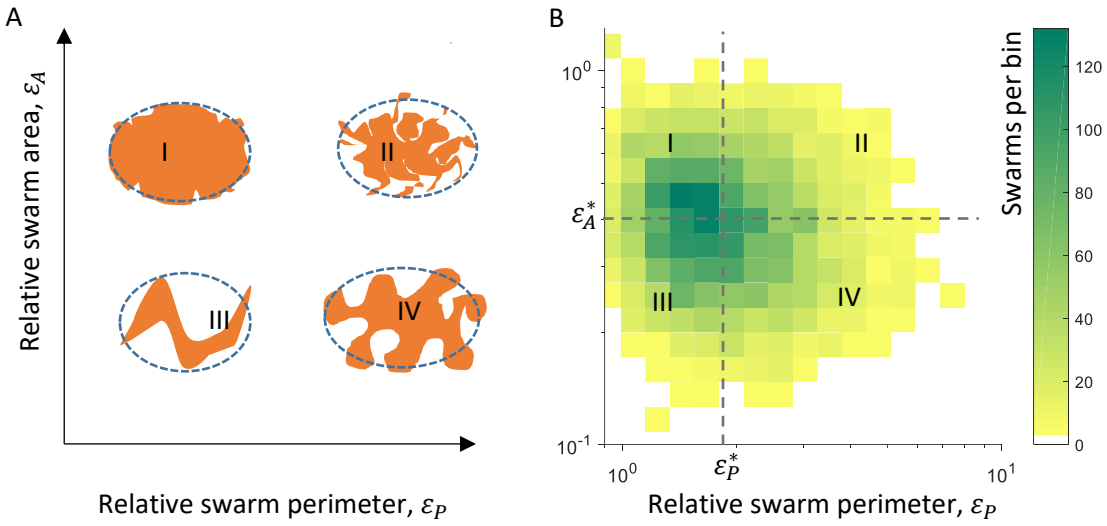
A
Relative swarm area, ε_A
I
II
III
IV
Relative swarm perimeter, ε_P
B
10^0
10^{-1}
ε_A^*
ε_P^*
10^0
10^1
I
II
III
IV
Relative swarm perimeter, ε_P
Swarms per bin
120
100
80
60
40
20
0

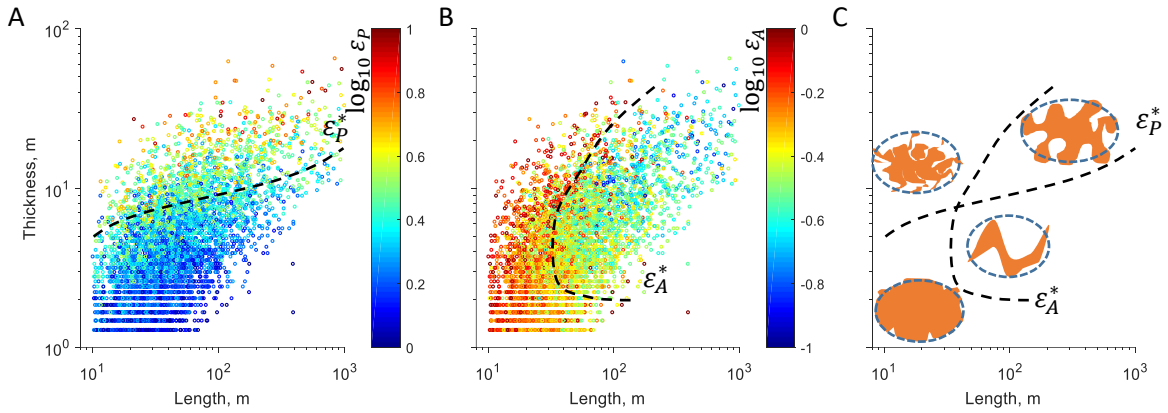
A
B
C
Thickness, m
Length, m
Length, m
Length, m
$\log_{10}\varepsilon_P$
$\log_{10}\varepsilon_A$
ε_P^*
ε_A^*
ε_P^*
ε_A^*